Internal reflection beneath capillary water waves: a method for measuring wave slope

J. R. Saylor

Ray-tracing simulations were performed to explore total internal reflection of light rays beneath capillary water waves. A vertically oriented light ray, scanned laterally below the wave surface, is mapped to a position that oscillates at a frequency f. It was found that f varies over 2 orders of magnitude as the dimensionless wave height a/λ varies from 0.34 to 0.73. This presents a possible frequency domain method for wave slope measurement in wave tank experiments. A linear relationship between the maximum displacement of the mapped ray and a/λ is also demonstrated for a/λ between 0.54 and 0.73, presenting a second wave slope measurement approach. The consequences of partial internal reflection are considered.

Key words: Wave slope measurement, internal reflection, capillary waves.

1. Introduction

The waves that populate the air–water interface play an important role in how water and air currents interact at the surface of oceans, lakes, and rivers. Waves affect the degree to which dissolved gases and heat are transferred from the air to the water and vice versa. Furthermore, water waves affect the scattering of microwave radiation, and therefore an understanding of water waves is relevant to the remote sensing of the ocean by way of microwave radars.

Capillary waves are of special interest with respect to the aforementioned phenomena. These waves, whose wavelengths are less than 2 cm, have slopes significantly larger than for longer wavelength gravity waves. Crapper[1] demonstrated that the dimensionless wave amplitude a/λ, where a is the peak-to-trough distance and λ is the wavelength, has a limiting value of $a/\lambda = 0.730$ for capillary waves, whereas the peak value for gravity waves is $a/\lambda = 0.142$.[2] Hence capillary waves can exhibit much steeper slopes than gravity waves. This larger slope increases the area of the air–water interface, enhancing the transport of heat, momentum, and mass. In addition to this area-enhancing effect, Szeri[3] has shown that capillary waves exhibit an additional increase in gas transport that cannot be explained by area enhancement alone. This additional increase is related to the straining of fluid near the surface, which thins the surface boundary layers.

The fact that capillary waves are both small and steep makes their measurement especially difficult. Intrusive probes such as capacitance wave sensors do not perform satisfactorily in capillary waves because it is difficult to construct a sensor that is significantly smaller than the wavelength. Moreover, intrusive probes affect the wave geometry, and viscous drag around the probe modifies the velocity field below the wave surface. Finally, the meniscus that surrounds the probe can be a significant fraction of the wavelength for small-scale capillary waves, further decreasing the measurement accuracy of intrusive probes.

Several optical methods have been developed to measure wave slope and wave height. These methods fall into one of two general categories based on the physical principle by which the measurement is obtained: (i) reflective methods and (ii) refractive methods. Reflective methods use light reflected off the wave surface, which is sensed subsequently by a photodetector. The light source can be artificial, such as a laser located above the water surface, or the light source can be the Sun, when Sun glint is used to ascertain wave slope. The geometric relationship between the wave surface, the light source, and the detector is used to determine the wave height, the wave slope, or both. Reflective methods can be used to obtain wave slope at a point or over an area. An example of the use of reflection to obtain wave slope at a point is presented in Wu *et al.*,[4] and an example

The author is with the Naval Research Laboratory, 4555 Overlook Avenue, S.W., Washington, D.C. 20375.

Received 2 May 1996; revised manuscript received 12 August 1996.0003-6935/97/061121-09$10.00/0

of the use of reflection to obtain wave slope over an area is presented in Cox and Munk,[5] where Sun glint is used as the light source.

Refractive methods utilize the angular displacement of light rays as they pass through an air–water interface to determine wave slope. The light source is typically a laser beam located on either the air side or the water side that is refracted at the air–water interface and detected on the opposite side of that interface. Examples of this type of method are presented in Lange *et al.*,[6] Tober *et al.*,[7] Sturm and Sorrell,[8] and Hughes *et al.*[9] Cox[10] developed a refractive imaging method wherein a flat object of varying color or intensity is placed below the water surface. A camera is placed above the water, and the color or intensity of light recorded on the image plane of the camera is related to the slope of the wave. A description of this method is presented in Zhang and Cox.[11] This method has the advantage of yielding a two-dimensional wave slope field instead of a wave slope at a single point. Images of the wave slope field can also be obtained by way of the refractive method by rastering a laser beam over a two-dimensional region. This technique is described by Hwang *et al.*[12] and also by Hara *et al.*[13]

The methods described above can be used in both wave tank studies and in open-sea measurements. However, the requirements for these two experimental environments are quite different. In the open sea the orientation of the slope gauge with respect to the gravity vector can change, and care must be taken to account for the moving measurement platform or to reduce its effect. Also the presence of foam, surfactants, bubbles, particulates, and droplets can lead to data dropout or erroneous measurements. Clearly, the open sea presents a much more challenging environment within which to conduct wave slope measurements. Accordingly, it is frequently desirable to perform measurements in a laboratory environment, such as a wave tank, where the variables that determine the wave characteristics can be controlled. A method for measuring wave slope is presented that is designed for such an environment, where the presence of surfactants and bulk-water contaminants can be controlled. The modifications that are necessary to utilize the proposed method in an open-sea environment are not discussed here, and it is assumed that the air and the water are free of surfactants and other contaminants.

All refractive measurements of wave slope are limited to a critical wave slope, above which a measurement cannot be obtained. This critical wave slope occurs when the angle between the light ray and the normal to the air–water interface exceeds the critical angle β_c, defined by Snell's law, resulting in total internal reflection of the ray. For the interface between air and water, in the absence of surfactants and contaminants, $\beta_c = 48.6°$ (different critical angles are observed in water containing substances that change the index of refraction, e.g., seawater). Because large amplitude capillary waves can exhibit slopes that vary from 0 to ∞ (see Fig. 1), the total internal reflection limitation is a significant impediment, and a method wherein waves of large slope can be measured is highly desirable. The method proposed herein actually utilizes total internal reflection of light rays to its advantage. As demonstrated here, a vertically oriented light ray that is internally reflected by the wave is mapped to a location on the floor of a wave tank (or on an imaginary plane at some location below the surface), which depends on the initial x location of the light ray. Thus if a laser beam is scanned laterally below the wave surface, the position of the mapping oscillates. This same effect will occur if the laser beam is fixed and the waves propagate past at a given velocity. A detector located at a fixed position on the tank floor can sense a periodic pulse of light as the light ray passes by. As demonstrated here, the frequency with which this ray passes the detector can be related to the wave slope, giving one the ability to measure wave slope in the frequency domain.

In Section 2 the ray-tracing method is described and the solutions for the wave profiles that are used to test the method are presented. The results are presented in Section 3, and Section 4 contains a discussion of these results and their limitations. A summary is presented in Section 5.

2. Problem Formulation

To explore the dynamics of internal light reflection below capillary waves, a solution for wave height as a function of space is needed. The solution derived by Crapper[1] is an exact, nonlinear solution for two-dimensional progressive capillary waves of arbitrary amplitude. This is an inviscid solution, and so the wave profiles are somewhat idealized. However, for the purpose of exploring the use of internal light reflection as a wave slope measurement technique, these waves are adequate. Crapper's solution is given in terms of the parameter α, which is defined as $\alpha = \phi/c\lambda$, where ϕ is the velocity potential and c is the phase velocity of the wave. The solution is

$$x/\lambda = \alpha - \frac{2}{\pi}\frac{A \sin 2\pi\alpha}{1 + A^2 + 2A \cos 2\pi\alpha}, \tag{1}$$

$$y/\lambda = \frac{2}{\pi} - \frac{2}{\pi}\frac{1 + A \cos 2\pi\alpha}{1 + A^2 + 2A \cos 2\pi\alpha}, \tag{2}$$

where

$$A = \frac{2\lambda}{\pi a}\left[\left(1 + \frac{\pi^2 a^2}{4\lambda^2}\right)^{1/2} - 1\right], \tag{3}$$

and y is positive in the downward direction. Solutions for the surface profile were obtained by varying α from 0 to 1, which spans a single wavelength.

Plots of the wave profiles for five different values of a/λ are presented in Fig. 1. The largest value of a/λ presented is 0.73, which represents the limiting height for a Crapper wave. Beyond this value, bubble entrainment or droplet formation occurs, phe-

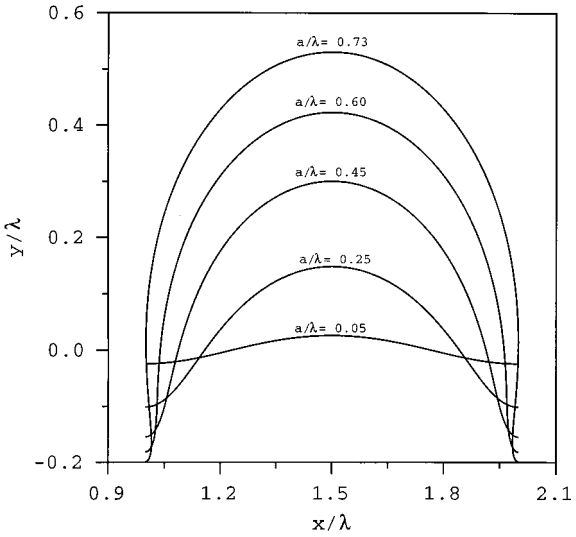

Fig. 1. Capillary wave profiles obtained from Crapper's solution for $a/\lambda = 0.05$, 0.25, 0.45, 0.60, and 0.73. The $a/\lambda = 0.73$ solution represents the highest wave that can exist without the entrainment of bubbles.

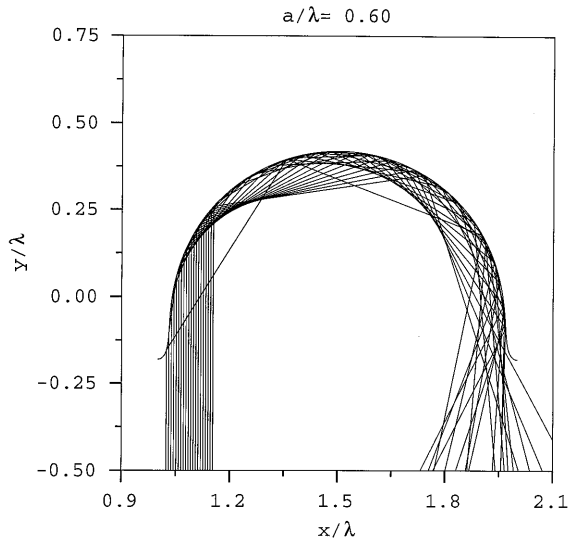

Fig. 3. Trajectories of 19 vertically oriented light rays interacting with a capillary wave with a height of $a/\lambda = 0.60$. The initial positions of the light rays are clustered within the region where total internal reflection occurs.

nomena not described accurately by the solution and not considered here.

In the research presented here, values of a/λ from 0.340 to 0.730 are considered. The rationale for the choice of the lower bound of a/λ is the following. For $a/\lambda < 0.2875$, the slope along the wave is sufficiently small that, at every point, a vertically oriented light ray will penetrate the air–water interface without total internal reflection. For $0.2875 \leq a/\lambda < 0.335$, vertically oriented light rays experience total internal reflection at certain points in the domain, but ultimately penetrate the air–water interface after one or more reflections. It is only for $a/\lambda > 0.335$ that vertically oriented light rays are reflected downward below the wave surface. Because it is this situation that is of interest here, only values of $a/\lambda > 0.34$ are considered. We note that although total internal reflection occurs only at locations where the critical angle is exceeded, partial internal reflection occurs at all locations along the wave. The effect of partial internal reflection on the results is discussed in Section 4.

To illustrate the process of ray penetration and total internal reflection, four wave profiles are plotted in Figs. 2(a)–2(d). In each figure, the trajectory of nine rays, equally spaced along the left half-wavelength, are plotted. In Fig. 2(a) $a/\lambda = 0.25$, and every ray passes through the air–water interface without reflection. In Figs. 2(b)–2(d), however, $a/\lambda > 0.35$, and in certain regions of the wave the rays experience total internal reflection. After two or more reflections, these rays follow a trajectory pointing downward below the wave surface. Even for large a/λ, total internal reflection occurs only when the input rays originate within a specific band of x locations. This band varies slightly with a/λ, but is located approximately within $1.02 < x/\lambda < 1.16$. In Fig. 3, the plot presented in Fig. 2(c) is replicated, with a high density of input rays clustered within this input band. This figure illustrates how equally spaced input rays experience total internal reflection and are then mapped to output positions that oscillate back and forth in a seemingly unpredictable manner. This phenomenon is further explored in Section 3.

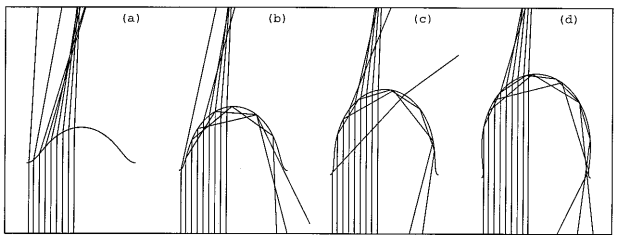

Fig. 2. Trajectories of vertically oriented rays interacting with four different capillary waves: (a) $a/\lambda = 0.25$, (b) $a/\lambda = 0.45$, (c) $a/\lambda = 0.60$, (d) $a/\lambda = 0.73$.

A ray-tracing algorithm was developed to study the behavior of internally reflected rays below the wave surface. At each value of a/λ, a vertical ray was traced from an initial x location, x_{in}. If the ray passed through the air–water interface, it was discarded. However, if the ray experienced total internal reflection, its path was traced through all of its reflections onto a final x position, x_{out}, on a plane below the wave surface located at $y = y_0$. An arbitrary value of $y_0 = 5\lambda$ was chosen, but other values could have been used with similar results. The value of x_{in} was then incremented, and the process was repeated until x_{in} was swept through an entire half-wavelength. A total of 1900 values of x_{in}, equally spaced over one half-wavelength, were considered for each value of a/λ. The x_{out} versus x_{in}

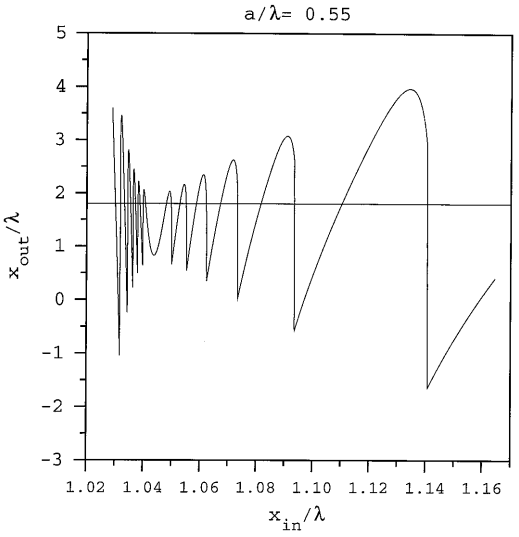

Fig. 4. Output x position x_{out}/λ of internally reflected rays versus their initial input positions x_{in}/λ for a wave of $a/\lambda = 0.55$. The horizontal line represents $x_{out} = x_c$.

information was stored for all 1900 rays. This entire process was then repeated for a new value of a/λ. The value of a/λ was increased in increments of 0.0006 until the entire a/λ range was considered.

3. Results

A sample plot of the x_{out} versus x_{in} data for $a/\lambda = 0.55$ is presented in Fig. 4. This plot reveals the oscillating nature of the mapped light ray x_{out} as x_{in} is scanned. A range of x_{in} from 1.02 to 1.16 is plotted. As mentioned above, outside of this range light rays do not experience total internal reflection. Another plot of x_{out} versus x_{in} is presented in Fig. 5 for $a/\lambda = 0.60$. Clearly, the oscillation frequency is much larger for $a/\lambda = 0.60$ than for $a/\lambda = 0.55$, showing

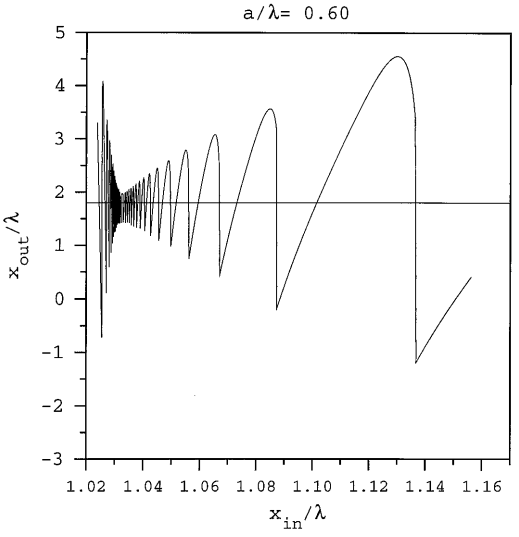

Fig. 5. Output x position x_{out}/λ of internally reflected rays versus their initial input positions x_{in}/λ for a wave of $a/\lambda = 0.60$. The horizontal line represents $x_{out} = x_c$.

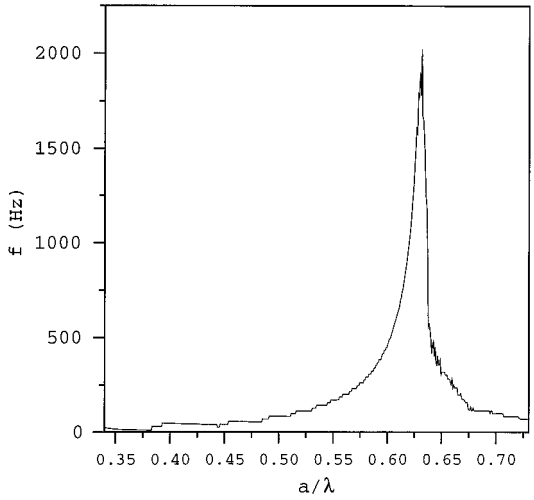

Fig. 6. Plot of x_c crossing frequency f versus a/λ. The peak resides at $a/\lambda = 0.63$. The value of x_c is 1.80λ.

that a small change in a/λ results in a dramatic change in the oscillation frequency of x_{out}.

To quantify this change in oscillation frequency, a crossing position $x_{out} = x_c$ was selected, and the average frequency f at which x_{out} crossed x_c was computed assuming a value of unity for the velocity at which the input ray x_{in}/λ was swept laterally across the domain. A value of $x_c = 1.8\lambda$ was selected to maximize the number of times x_{out} crossed x_c. A horizontal line is drawn at $x_{out} = x_c$ in Figs. 4 and 5.

Figure 6 presents a plot of f versus a/λ. The plot shows a monotonic increase in f to a value of $a/\lambda = 0.63$, after which f drops rapidly with a/λ. The significance of these results, and how they can be used to measure wave slope, is discussed in Section 4. The steps in the plot of f versus a/λ, presented in Fig. 6, are not attributable to insufficient resolution in a/λ, but rather to the way in which f is computed. Here f is simply the inverse of the average distance between points where x_{out} crosses x_c. The number of times that this crossing occurs is small when a/λ is small, and even for large a/λ it is never greater than 250. Because the number of x_c crossings must, by definition, increase in discrete units, f also increases discretely, giving the f versus a/λ plot the somewhat noisy appearance observed in Fig. 6. Use of a fast Fourier transform algorithm to compute an average frequency for the x_{out} versus x_{in} signals most likely would remove the jagged appearance of Fig. 6; however, the difference would be subjective and would not affect the conclusions drawn herein.

4. Discussion

The plot of f versus a/λ presented in Fig. 6 shows that f is highly sensitive to a/λ. The magnitude of f varies by 2 orders of magnitude over the range of a/λ considered. For Crapper waves, knowledge of a/λ permits a complete reconstruction of the wave profile, and therefore the wave slope at all points along the wave is known once a/λ is determined. A schematic illustration of an experimental setup for measuring f

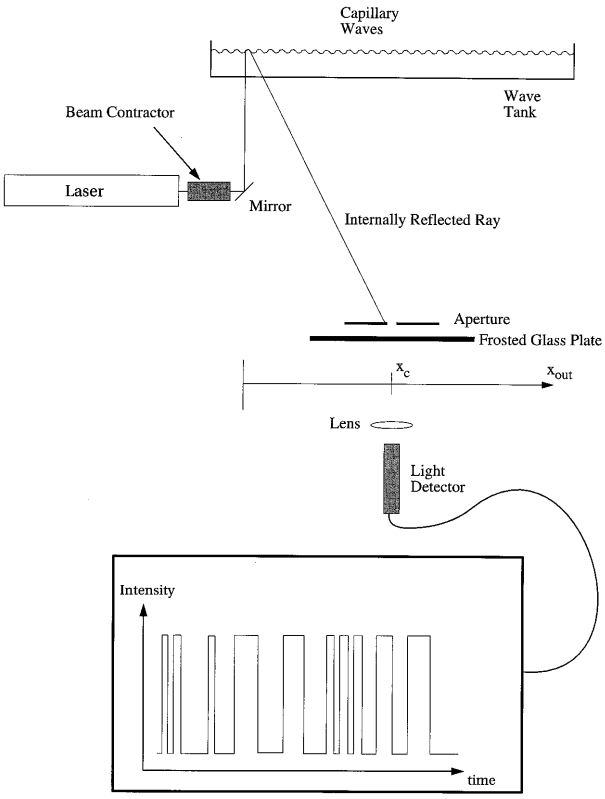

Fig. 7. Schematic illustration of experimental setup for the proposed wave slope measurement technique.

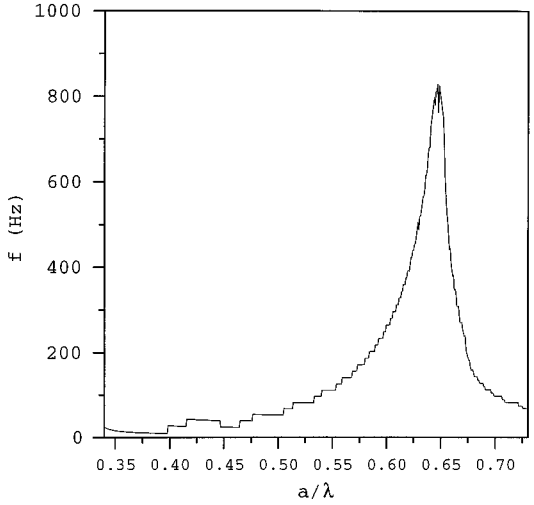

Fig. 8. Plot of x_c crossing frequency f versus a/λ. The peak resides at $a/\lambda = 0.65$. The value of x_c is 2.20λ.

is presented in Fig. 7. In this schematic, the reflected light ray strikes a frosted glass plate. A lens is placed between the frosted glass and a photodetector (e.g., photomultiplier tube, silicon photodiode, etc.) so that the plane of the frosted glass surface is focused onto the surface of the photodetector. An aperture whose center is located at $x = x_c$ is placed in front of the frosted glass so that the photodetector sees light only when the laser beam is mapped to the position $x_{\text{out}} = x_c$. Prior to striking the capillary wave, the laser beam passes through a beam contractor that is used to reduce the diameter of the laser beam and therefore increase the spatial resolution of the system. The required resolution imposed by the small size of the capillary waves will be discussed later in this section. With the setup configured in this fashion, a light ray moving across the frosted glass plate would result in a pulse train as the photodetector output. The average frequency of the pulse train f could be obtained in real-time with a fast Fourier transform analyzer or by storing the detector output and processing the signal after the conclusion of the experiment.

This method assumes a/λ is known once f is measured. The f versus a/λ plot presented in Fig. 6 has a peak, and hence for each measured value of f there are two possible values of a/λ. There are two ways to circumvent the problem posed by this degeneracy. The peak in Fig. 6 occurs for $a/\lambda = 0.63$. This actually corresponds to large amplitude waves that are not observed in many cases. Hence the degeneracy in Fig. 6 can be avoided if it is known *a priori* that the maximum a/λ will be less than 0.63. Alternately, the problem can be avoided by an appropriate choice of x_c. In the results presented to this point, x_c was set to 1.8λ because, in an approximate sense, the number of x_c crossings was maximized for most values of a/λ. However, for each value of a/λ, the value of x_c for which the number of x_c crossings is maximized is different. In fact, as a/λ increases, this optimum x_c value continually increases. Because of this increase, some x_c crossings are missed in regions where the x_{out} signal does not cross x_c. This is part of the reason why f decreases for $a/\lambda > 0.63$ in Fig. 6 (the other part of the reason is that the overall signal frequency decreases). Hence, by varying x_c a means can be provided for tuning the position of the peak in Fig. 6. Increasing x_c moves the peak to a higher value of a/λ, thereby moving the region where degenerate values exist to a higher a/λ. This is physically simple to do, because varying x_c can be achieved by moving the x location of the aperture. In Fig. 8, a plot of f versus a/λ is presented for $x_c = 2.20\lambda$, illustrating a shift in the peak to $a/\lambda = 0.65$.

The x_{out} behavior observed in Figs. 4 and 5 and the resulting frequency behavior observed in Figs. 6 and 8 are due to total internal reflection, which occurs when the angle between the incident ray and the normal to the air–water interface is greater than the critical angle β_c. However, for angles less than β_c there is partial internal reflection of light rays, which also contributes to the detector signal. The reflectance of the air–water interface R is governed by the Fresnel laws of reflection:

$$R = \frac{1}{2}\left[\frac{\sin^2(\beta - \beta')}{\sin^2(\beta + \beta')} + \frac{\tan^2(\beta - \beta')}{\tan^2(\beta + \beta')}\right], \qquad (4)$$

where β is the angle between the incident ray and the normal to the interface on the water side, and β' is the angle between the refracted ray and the normal

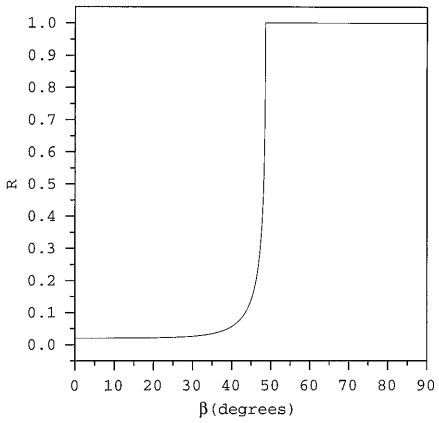

Fig. 9. Plot of reflectance R as a function of the angle β, which is the angle between the incident ray and the normal to the interface on the water side.

on the air side.[14] Here unpolarized light is considered, and R is the average of the parallel and perpendicular polarization reflectances. The angles β and β′ are related by Snell's law,

$$R = \frac{n}{n'} = \frac{\sin \beta'}{\sin \beta}, \tag{5}$$

where n and n' are the indices of refraction of water and air, respectively. A plot of R versus β is presented in Fig. 9, which demonstrates that, for $\beta > \beta_c$ (48.6°), $R = 1$ and R decreases rapidly with decreasing β for $\beta < \beta_c$. Because the results presented to this point considered only total internal reflection, the contribution of light reflected at $\beta < \beta_c$ was not included. The influence of partial internal reflection can be reduced by passing the detector signal through a thresholding circuit or by thresholding the data computationally after the data have been acquired. However, a certain amount of partial internal reflection will always be present. The effect of partial internal reflection is demonstrated in Figs. 10(a)–10(c), where plots of x_{out} versus x_{in} are plotted for the same a/λ value as in Fig. 4. In Fig. 10(a), the threshold is set to 50%, which means that partially reflected light having an intensity less than or equal to 50% of the total internal reflection intensity is included in the ray-tracing simulations. The differences between Figs. 10(a) and 4 are not discernible (note that the x_{in}/λ scales are slightly different). In Figs. 10(b) and 10(c), the threshold value is further reduced to 10% and 5%, respectively. Note that even at a 5% threshold, the signal is still quite similar to that in Fig. 4. The only difference between the signals in Figs. 10(a)–10(c) and 4 is that the minimum and maximum values of x_{in}/λ for which a ray is mapped to an x_{out} position increases. That is, the range of x_{in} for which a signal is observed increases. This is seen as a growth in the width of the signal in Figs. 10(a)–10(c). This growth negligibly affects the frequency of the signal because no new crossings of the $x = x_c$ position are introduced. This is demonstrated explicitly in Fig. 11 where the frequency versus a/λ data from Fig. 6 are replotted with the data that include partial internal reflection. The two curves are barely discernible, indicating that the presence of partial internal reflection gives results that are essentially identical to those obtained if one assumes that only total internal reflection is present.

The presentation of this method has, to this point, assumed implicitly an idealized light ray. That is, the light beam that is directed vertically upward from the floor of the wave tank is assumed to have an infinitesimally small diameter. Actual implementation of this method would utilize a laser beam of finite diameter that would introduce limitations in spatial resolution. Complete resolution of the oscillations in the x/λ data presented in Fig. 4, for example, would require a laser having a diameter smaller than the smallest oscillations, which are of the order of $x/\lambda = 0.003$. Although this is feasible for relatively long wavelength waves, resolution of a 1-mm wave, for example, would require a spatial resolution better than 3 μm. Focusing a laser beam to such a small diameter is not practically feasible. Moreover, focusing of a laser beam is not a solution because fo-

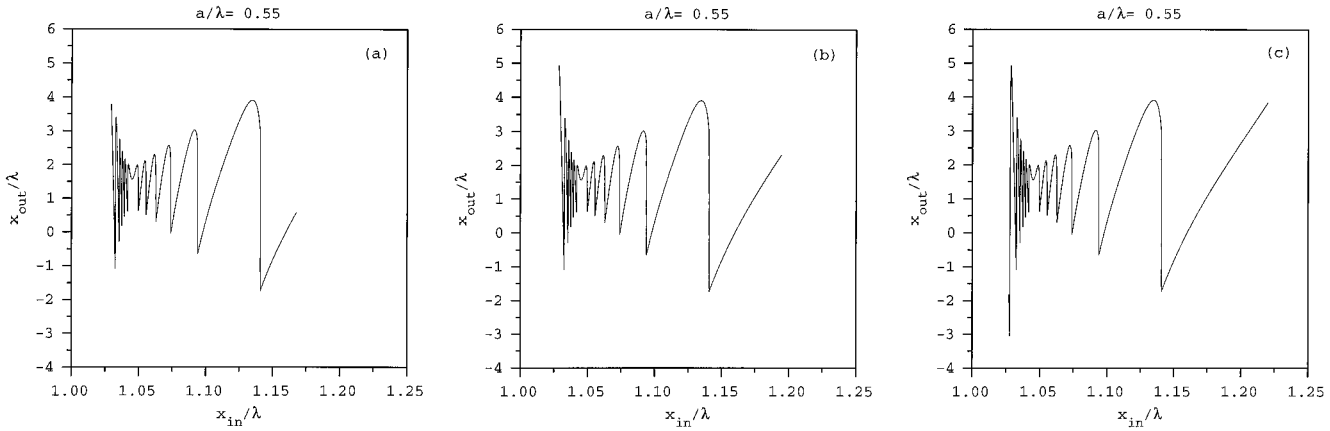

Fig. 10. Plots of x_{out} versus x_{in} at $a/\lambda = 0.55$, illustrating the effect of partial internal reflection. The reflectance threshold is set at (a) 50%, (b) 10%, (c) 5%.

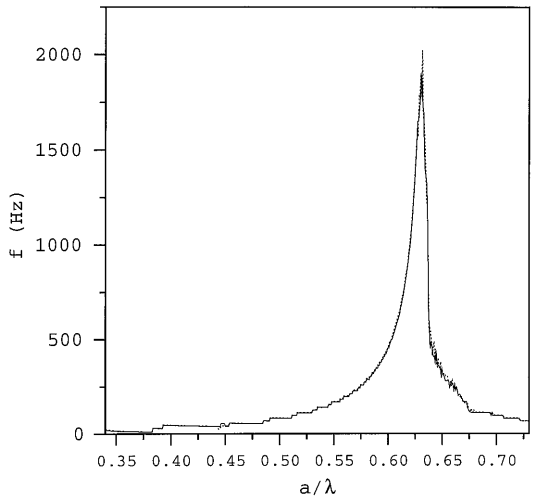

Fig. 11. Plots of frequency versus a/λ. The dotted curve is for total internal reflection only. The solid curve is for results obtained considering both total internal reflection and partial internal reflection with a threshold setting of 50%.

cusing changes the direction of the off-axis rays from the assumed vertical orientation, resulting in different off-axis rays being mapped to different x_{out} positions. A beam contractor, as illustrated in Fig. 7, could be used to shrink the diameter of the laser beam while maintaining the collimated nature of the light. However, contracting a laser beam to small diameters is also quite difficult.

If a laser beam is used that is larger than the scales over which x_{out}/λ varies, the photodetector illustrated in Fig. 7 would not observe a pulse train, but rather a continuously modulated signal that peaks when the center of the laser beam is located at an x_{in} position for which $x_{out} = x_c$. Laser beams typically exhibit a Gaussian intensity distribution $I(r)$:

$$I(r) = \frac{2P}{\pi\omega^2}\exp(-2r^2/\omega^2), \tag{6}$$

where P is the total laser power, ω is the $1/e^2$ radius of the beam, and r is the radial distance from the beam center line.[15] The photodetector output from a wave interrogated by a Gaussian laser beam would be the integration of Eq. (6) at each of the x_{in} points for which total internal reflection maps rays to $x_{out} = x_c$. That is, when the beam is centered at an x_{in} location where the resulting x_{out} position is equal to x_c, the tails of the Gaussian distribution would also pass over other x_{in} positions for which $x_{out} = x_c$. In this way the tails would contribute to the detector signal. Theoretically, the frequency of the resulting detector signal could still be related to the wave characteristics. However, because the detector signal would consist of a large dc signal superposed with a small oscillating component, the system would be sensitive to noise.

An alternate measurement technique for the case in which a sufficiently small laser beam cannot be attained is now presented. Figures 4 and 5 show

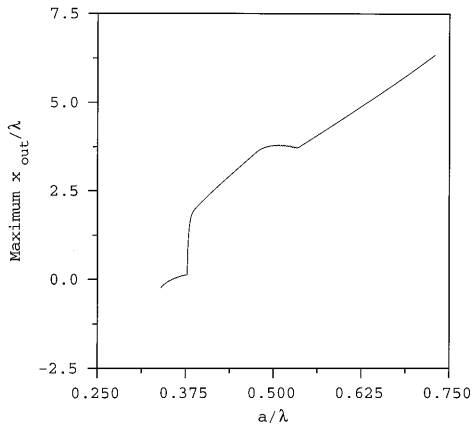

Fig. 12. Maximum values of x_{out}/λ versus a/λ.

that the maximum value of x_{out}/λ is larger for $a/\lambda = 0.60$ than for $a/\lambda = 0.55$. This observation is in fact a general result in the sense that the maximum value of x_{out}/λ increases with a/λ for all a/λ investigated. This is illustrated in Fig. 12 in which the maximum value of x_{out}/λ is plotted against a/λ. Figure 12 shows that the maximum value of x_{out}/λ not only increases with a/λ, but is also a linear function of a/λ for $0.54 < a/\lambda < 0.73$, an important result because this ray-tracing method is most useful at a high wave slope at which refractive methods fail. The effect of partial internal reflection on the maximum value of x_{out}/λ was tested and was found to have an insignificant effect on the data plotted in Fig. 12.

An experimental setup designed to exploit the aforementioned behavior is illustrated in Fig. 13. In this figure, the photodetector of Fig. 7 is replaced with a position sensitive detector (PSD), and the aperture is replaced with a half-aperture centered at $x = x_c$. The frosted glass plate and the lens have also been eliminated from this experimental setup. The half-aperture blocks all output rays on one side of x_c, allowing the PSD to see only values of x_{out} larger than x_c. PSD's yield an output signal that is related linearly to the location of the centroid of the light spot that is incident upon its surface. The maximum displacement of x_{out} can be observed, even if the laser beam is larger than the spatial scale over which oscillations in x_{out} are observed. Hence the maximum displacement of the centroid of the light spot incident upon the PSD can be related to a/λ after an appropriate calibration.

A drawback of the methods presented here is that *a priori* knowledge of the wave profile is required before the measured parameter (frequency or maximum x_{out} position) can be related to the wave slope. The Crapper waves simulated here represent a solution of the capillary wave profile for zero viscosity. A comparison of the ray-tracing characteristics of Crapper waves with those of real (viscous), high-amplitude capillary waves would be extremely useful. Unfortunately, we are unaware of any viscous, nonlinear solutions for capillary wave profiles. The existence of a viscous, nonlinear solution would

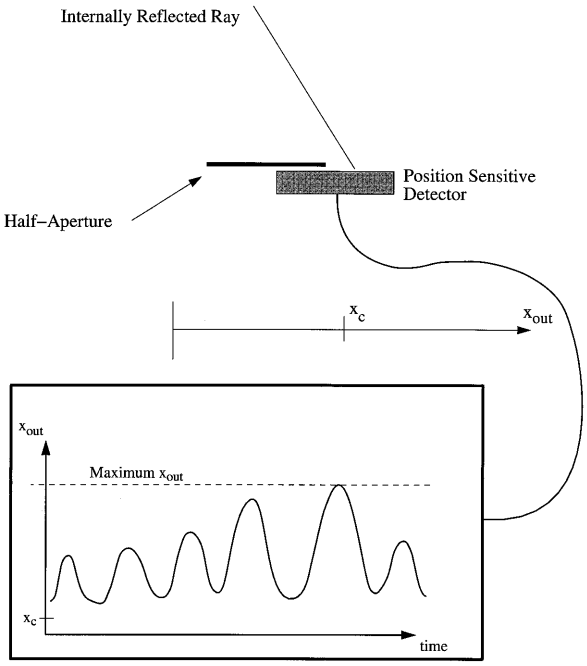

Fig. 13. Experimental setup for an alternate wave slope measurement technique.

make the proposed method immediately usable in the laboratory because the simulations performed here could be repeated to obtain the relationship between a/λ and f for the actual wave profiles. In the absence of such a solution, the proposed method must be first calibrated by obtaining wave profiles of capillary waves at several values of a/λ using digital imaging. This is a labor-intensive procedure; however, once performed, the empirical waveforms could be used to predict the ray-tracing characteristics of the waves, yielding an f versus a/λ (or maximum x_{out} versus a/λ) relationship that would serve as a calibration for the method. The need for this calibration limits the utility of this method in the open sea where an essentially unknown wave field consisting of many different wavelengths as well as unknown surfactants and contaminants are present. The method would be most useful in wave tank studies where controlled, repeatable wave fields are produced. Examples of this include investigations of parasitic capillary waves, such as those presented in Perlin *et al.*,[16] as well as studies of Faraday waves, such as those presented in Ciliberto and Gollub[17] and in Henderson and Miles.[18]

Even in the absence of the calibration described above, the proposed method is useful for measuring wave slope because a vertically oriented ray, such as a laser beam, will be reflected onto the floor of a wave tank only if the angle between the vertical and the normal to the wave exceeds the critical angle for total internal reflection at some point along the wave. In this way the method described here could be used in a simple yes and no mode to determine if a critical wave slope has been exceeded. It is also possible that experimental testing of the method may reveal x_{out} versus x_{in} behavior that is similar to that displayed in Figs. 4 and 5, indicating that the Crapper wave profile is a reasonable approximation of actual capillary waves. Future research in this direction is planned.

5. Conclusion

Ray-tracing simulations beneath the surface of Crapper waves were performed to test the use of total internal reflection as a method for measuring wave slope in high-amplitude capillary waves. The simulations revealed that, as a capillary wave passes over a vertically oriented laser beam, the internally reflected ray traces a path on a plane below the wave surface that oscillates at a frequency f. For $0.34 < a/\lambda < 0.73$, f varies over 2 orders of magnitude, making this oscillation frequency a sensitive measure of wave slope. The measurement also has the advantage of being performed in the frequency domain. It was also demonstrated that the maximum displacement of the reflected ray is a function of a/λ and that this relationship is linear for $0.54 < a/\lambda < 0.73$. This latter method has the ability to measure wave slope when adequate spatial resolution is not available. Partial internal reflection did not have a significant effect on the behavior of either method. The ray-tracing results presented here are particularly promising because they excel at high values of a/λ, exactly the region in which existing techniques fail. Future research will focus on imaging the profiles of high-amplitude capillary waves to be used in the calibration of this method.

This research was performed while the author held a National Research Council–Naval Research Laboratory Postdoctoral Research Associateship.

References

1. G. D. Crapper, "An exact solution for progressive capillary waves of arbitrary amplitude," J. Fluid Mech. **2,** 149–159 (1957).
2. J. H. Michell, "The highest waves in water," Philos. Mag. **5,** 430 (1893).
3. A. J. Szeri, "Capillary waves and air-sea gas transfer," J. Fluid Mech. (1997).
4. J. Wu, J. M. Lawrence, E. S. Tebay, and M. P. Tulin, "A multiple purpose optical instrument for studies of short steep water waves," Rev. Sci. Instrum. **40,** 1209–1213 (1969).
5. C. S. Cox and W. Munk, "Statistics of the sea surface derived from sun glitter," J. Marine Res. **13** (3), 198–227 (1954).
6. P. A. Lange, B. Jähne, J. Tschiersch, and I. Ilmberger, "Comparison between an amplitude-measuring wire and a slope-measuring laser water wave gauge," Rev. Sci. Instrum. **53,** 651–655 (1982).
7. G. Tober, R. C. Anderson, and O. H. Shemdin, "Laser instrument for detecting water ripple slopes," Appl. Opt. **12,** 788–794 (1973).
8. G. V. Sturm and F. Y. Sorrell, "Optical wave measurement technique and experimental comparison with conventional wave height probes," Appl. Opt. **12,** 1928–1933 (1973).
9. B. A. Hughes, H. L. Grant, and R. W. Chappell, "A fast response surface-wave slope meter and measured wind-wave moments," Deep-Sea Res. **24,** 1211–1223 (1977).
10. C. S. Cox, "Measurement of slopes of high-frequency wind waves," J. Marine Res. **16,** (3), 199–225 (1958).

11. X. Zhang and C. S. Cox, "Measuring the two-dimensional structure of a wavy water surface optically: a surface gradient detector," Exp. Fluids **17,** 225–237 (1994).
12. P. A. Hwang, D. B. Trizna, and J. Wu, "Spatial measurements of short wind waves using a scanning slope sensor," Dyn. Atmos. Oceans **20,** 1–23 (1993).
13. T. Hara, E. J. Bock, and D. Lyzenga, "In situ measurements of capillary-gravity wave spectra using a scanning laser slope gauge and microwave radars," J. Geophys. Res. **99,** 12,593–12,602 (1994).
14. F. A. Jenkins and H. E. White, *Fundamentals of Optics* (McGraw-Hill, New York, 1957).
15. A. C. Eckbreth, *Laser Diagnostics for Combustion Temperature and Species* (Abacus, Cambridge Mass., 1988).
16. M. Perlin, H. Lin, and C-L. Ting, "On parasitic capillary waves generated by steep gravity waves: an experimental investigation with spatial and temporal measurements," J. Fluid Mech. **255,** 597–620 (1993).
17. S. Ciliberto and J. P. Gollub, "Chaotic mode competition in parametrically forced surface waves," J. Fluid Mech. **158,** 381–398 (1985).
18. D. M. Henderson and J. W. Miles, "Single-mode Faraday waves in small cylinders," J. Fluid Mech. **213,** 95–109 (1990).